THE JOURNAL OF PHYSICAL CHEMISTRY B

Article

Cite This: J. Phys. Chem. B 2019, 123, 2432−2438

pubs.acs.org/JPCB

Experimental Evidence for a Cluster Glass Transition in Concentrated Lysozyme Solutions

Maxime J. Bergman,[†] Tommy Garting,[†] Peter Schurtenberger,[†,‡] and Anna Stradner*[,†,‡]

[†]Division of Physical Chemistry, Department of Chemistry, Lund University, PO Box 124, SE-22100 Lund, Sweden

[‡]LINXS - Lund Institute of advanced Neutron and X-ray Science, SE-22100 Lund, Sweden

Supporting Information

ABSTRACT: Lysozyme is known to form equilibrium clusters at pH ≈ 7.8 and at low ionic strength as a result of a mixed potential. While this cluster formation and the related dynamic and static structure factors have been extensively investigated, its consequences on the macroscopic dynamic behavior expressed by the zero shear viscosity η_0 remain controversial. Here we present results from a systematic investigation of η_0 using two complementary passive microrheology techniques, dynamic light scattering based tracer microrheology, and multiple particle tracking using confocal microscopy. The combination of these techniques with a simple but effective evaporation approach allows for reaching concentrations close to and above the arrest transition in a controlled and gentle way. We find a strong increase of η_0 with increasing volume fraction ϕ with an apparent divergence at $\phi \approx 0.35$, and unambiguously demonstrate that this is due to the existence of an arrest transition where a cluster glass forms. These findings demonstrate the power of tracer microrheology to investigate complex fluids, where weak temporary bonds and limited sample volumes make measurements with classical rheology challenging.

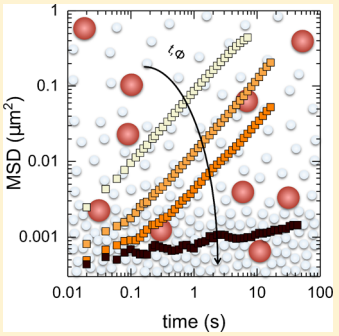

INTRODUCTION

At low ionic strength, the globular protein lysozyme has shown to interact via a mixed potential that consists of a long-range screened Coulomb repulsion and a short-range attraction (SALR potential), leading to the formation of equilibrium clusters at higher protein concentrations.[1] The current and generally accepted picture is that such a SALR potential leads to equilibrium cluster formation as a generic feature that can be found in a large number of vastly different synthetic and biological colloidal systems, and it has, for example, serious implications in biologics, i.e., for formulations of biological macromolecules such as antibodies or globular proteins.[2,3] Moreover, aggregating proteins interacting via the SALR potential have been linked to various degenerative diseases, such as sickle cell disease.[4,5]

The structural and dynamic consequences of this cluster formation have been discussed in a vast number of publications, where analogies to colloids have been used to understand and predict the relevant experimental parameters, such as primarily the static structure factor, as well as the short and long time collective and self-diffusion coefficients.[6−18] Here it has been realized that self-assembly into clusters can considerably enhance the viscosity of these solutions at higher concentrations. There have in fact been experimental and simulation studies that discussed the existence of a cluster-induced dynamical arrest or a cluster glass, but this topic has remained controversial, with conflicting evidence so far.[14,17,19]

Given the enormous attention devoted to equilibrium cluster formation in proteins and colloids, and the well-documented importance of the process also for applications such as drug formulation, there is in fact an astonishing lack of publications investigating its effects on macroscopic flow properties. This unsatisfactory situation clearly is not only caused by the notoriously difficult task of measuring protein solution viscosities with traditional rheological tools,[14] but also due to the experimental difficulties in preparing samples with sufficiently high concentrations.

In fact, only two experimental studies discuss the formation of a cluster glass and report on the zero-shear viscosity behavior of lysozyme beyond $\phi = 0.25$, but they arrive at completely different conclusions. One study[14] found indications of a macroscopic arrest ($\phi_g \gtrsim 0.26$ at 5 °C) while the other[17] concluded that lysozyme does not arrest macroscopically; although a slowing down of dynamics was found on short time scales, rheology revealed Newtonian fluid behavior even at $\phi = 0.345$ at 5 °C.

In this work, we therefore aim to further investigate the possible existence of a cluster glass transition in highly concentrated lysozyme samples and thus revisit the viscosity-concentration dependency. In order to probe such samples close to the glass transition, we resort to the field of microrheology. Passive microrheology is a noninvasive technique that relies on thermal motion and thus indirectly measures the zero shear viscosity, η_0, of a sample by tracking the motion of embedded tracer particles.[20,21] The use of microrheology leads to an elegant experimental design, where a

Received: December 6, 2018
Revised: February 14, 2019
Published: February 20, 2019

DOI: 10.1021/acs.jpcb.8b11781
J. Phys. Chem. B 2019, 123, 2432−2438

mere ~150 μL of a specific lysozyme sample can be used in two different experimental setups. The first, tracer particle microrheology based on dynamic light scattering (DLS), has previously been successfully used on moderately concentrated lysozyme solutions[22−25] in order to prove the efficacy of the technique. The second technique is (passive) multiple particle tracking (MPT), facilitated by confocal laser scanning microscopy (CLSM). This technique is conventionally used for determining rheological properties of complex fluids[26−28] and has already been applied to moderately concentrated lysozyme solutions[22] as a proof of concept.

In addition, we develop and apply a simple evaporation process in order to create lysozyme solutions with volume fractions beyond $\phi = 0.35$ in a controlled way. This allows us for the first time to unambiguously confirm the existence of a cluster glass transition in lysozyme solutions at low ionic strength. We discuss our findings in the context of the existing experimental data and relate them to new and recently published simulation results.[14,17,19]

MATERIALS AND METHODS

Tracer Particle Modification. Fluorescently labeled carboxylate modified polystyrene (PS) particles with a diameter of 0.2 μm were purchased from Thermo-Fisher (F8809). Particles were dialyzed before surface modification to remove any nonionic surfactants present from manufacturing. The surface modification has been discussed in detail earlier,[25] however it will be described briefly here. Using an amine-coupling reaction, amine-PEG (poly(ethylene glycol)) brushes were covalently bound to the carboxyl groups on the PS particles. The amine-PEG, with molecular weight 20 kDa, was purchased from Rapp Polymere (1220000-2) and used as received. Amine-PEG in a pH 6.0 MES-buffer was mixed with particles at a 50× excess of amine-PEG to carboxyl groups. The cross-linker, *N*-(3-(dimethylamino)propyl)-*N*′-ethylcarbodiimide, was added at a concentration of 20 mM with the buffer finally adjusted to acidic pH using a 0.1 M MES-solution. The mixture was left for 24h after which the reaction was aborted by the addition of glycine. The now pegylated particles were washed and retrieved using centrifugation with the first incomplete pellet being discarded to remove larger particles that were already present in the original particle dispersion as received.

Sample Preparation. The procedure for preparing lysozyme samples has been described earlier.[1,14,25] Lysozyme, lyophilized powder from Sigma-Aldrich (L6876), was dissolved in salt-free 20 mM Hepes buffer, pH 7.8, at a concentration of 40 mg/mL. Because of the presence of salt in the purchased lysozyme powder, it was subsequently washed thoroughly using a 15 mL 3 kDa Amicon Ultra centrifugal filter by replacing the buffer until the conductivity of the supernatant was that of the native buffer. The lysozyme was further concentrated using the same devices with the final higher concentrations achieved using 0.5 mL 10 kDa Amicon Ultra centrifugal filters. This allowed for sample volumes of ~100−300 μL which are more than sufficient for microrheology measurements. The final sample concentration was determined using UV−vis spectrometry with ${}^{1\%}_{1\ \mathrm{cm}}\epsilon_{280\ \mathrm{nm}} = 2.64$ and converted to volume fraction, ϕ, using a voluminosity of 0.74 mL/g.[14,25] The highest volume fraction achievable using this method was $\phi = 0.35 \pm 0.03$.

Protein samples were mixed with the particle dispersion, at a particle concentration of ~10^{-2} wt%, using a vortexer and the accompanied change in concentration was recorded gravimetrically. Samples were prepared just before measurements and subsequently split into dynamic light scattering (DLS) and multiple particle tracking (MPT) parts.

Dynamic Light Scattering. A 3D modulated cross-correlation light scattering instrument (LS Instruments GmbH, Switzerland) was used in combination with a diode laser (λ = 660 nm) as the light source. The experimental setup is explained in detail elsewhere.[29−31] The DLS data was obtained for 3−20 min, depending on sample viscosity, at 90° where each measurement was repeated three times with approximately 100 μL used for each sample. Next, using a first order cumulant analysis,[32,33] the apparent diffusion coefficient, D, of the tracer particles is obtained and normalized against the protein-free case, thus yielding the relative zero shear viscosity, η_r, according to the Stokes−Einstein expression $D = \frac{k_B T}{6\pi\eta R_H}$, where k_B is the Boltzmann constant, T is temperature, R_H is the particle hydrodynamic radius, and η is the sample viscosity.[20,21] Verification of successful surface modification was initially determined by continuously investigating the apparent particle size using DLS at an angle of 90°, when dispersed in a 2 M NaCl solution. Lack of sufficient functionalization results in an apparent size increase due to aggregation. This is shown in Figure S1 in the Supporting Information where the apparent hydrodynamic radii of both functionalized and untreated particles are shown, normalized by their respective sizes in salt-free water, verifying that the functionalized particles are indeed sterically stabilized.

Confocal Microscopy. For image acquisition, an inverted confocal laser scanning microscope (CLSM) (Leica, DMI6000) with a SP5 tandem resonant scanner at 50 frames/s was used. An oil immersion objective (100×, n.a. 1.4) was used for all images and a HeNe laser with wavelength λ = 543 nm. Three to five videos of at least 8000 frames were recorded, with each frame 512 × 256 pixels or 51.67 × 25.83 μm. Each video was made at a different location in the sample and at 20 μm (≈100 particle diameters) depth from the coverslip to exclude wall interactions. Because of the low concentration of particles, such deep penetration of the sample is possible. The setup includes a temperature-controlled box around the entire microscope, allowing for temperature control ±0.2 °C. Samples were equilibrated at least 20 min before measuring at 20 °C. The sample cell consists of a microscopy slide with a double sided sticker (Secure-Seal spacer, 9 mm diameter, 0.12 mm deep) which was sealed with a coverslip. All glass slides and coverslips were cleaned and dried before use.

Particle tracking was performed using the standardized image analysis routines in IDL from Crocker et al.[34] Instead of relating the slope of the resultant 2D mean squared displacement (MSD) to the particle diffusion coefficient, we followed the approach as described by Josephson et al.[35] In short, the one-dimensional Van Hove self-correlation for each specific lag time τ was calculated for both x and y direction. The Van Hove self-correlation function $P(\Delta x, \tau)$ describes the probability of a particle moving Δx after a certain lag time τ. Such a distribution of displacements follows a Gaussian distribution with enough statistics if purely diffusive particles experience a homogeneous environment.[36] We tested for which lag times τ the shape of the Van Hove function indicated a purely diffusive system, and took only the displacement data Δx at the specific time point with highest statistics. These displacements were then used to calculate the tracer diffusion

DOI: 10.1021/acs.jpcb.8b11781
J. Phys. Chem. B 2019, 123, 2432−2438

coefficient D via the Stokes−Einstein relation. With decreased particle mobility, the systematic errors in experimental settings and particle tracking become more important. For this reason, the diffusion coefficient was also calculated using $P(\Delta y, \tau)$ to increase statistics.

In order to get an idea of the limitations of our confocal setup, we measured the apparent motion of the tracer particles immobilized in a cross-linked matrix of PNIPAM. The same settings were used as before and as a result, we determined our noise floor (i.e., the maximum displacement that can be detected) to be around $\langle r^2 \rangle \sim 0.002\ \mu m^2$. The noise floor (shown as a solid black line in Figure 3) also highlights the apparent motion at long lag times arising from drift, which inherently has a larger effect on the MSD at long lag times since $\langle x^2 + y^2 \rangle = 4D\tau + (V\tau)^2$, where V is the overall velocity of the sample.[37] Although we attempted to remove drift, it was not eliminated completely.

RESULTS AND DISCUSSION

The resulting relative (zero shear) viscosity, $\eta_r = \eta_{Sample}/\eta_{Solvent}$, obtained from DLS-microrheology, is shown in Figure 1 as a function of volume fraction, ϕ. The data is in good agreement with earlier findings,[14,25] suggesting indeed the previously postulated existence of a cluster glass transition. DLS measurements using nonfluorescent tracer particles[25] yield the same result and confirm that the fluorophores do not negatively influence DLS measurements.

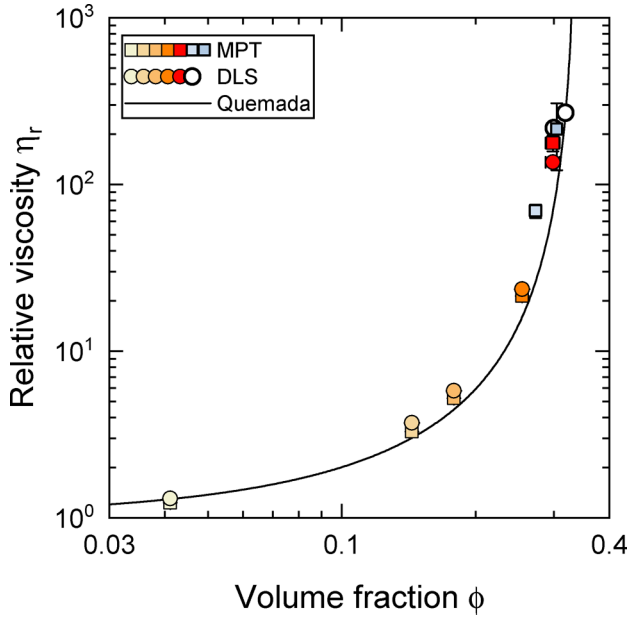

Figure 1. Relative viscosities of lysozyme solutions at 20 °C as obtained from DLS (circles) and MPT (squares) agree well over a wide concentration regime (colored yellow−red). Two reference samples with nonfluorescent tracer particles investigated using DLS are also included (white circles) to demonstrate that the presence of fluorophores does not negatively impact the DLS results. Note that for clarity only a subset of the data is shown in this graph while the entire set is presented in the Supporting Information, Figure S2. A Quemada fit to the entire set of data yields a volume fraction of approximately 0.34 for the liquid−solid transition. The average relative viscosity of the two least concentrated samples from the evaporation series in Figure 3 (blue squares) agrees well with the conventionally prepared samples.

However, there remains the discrepancy with the study of Godfrin et al.,[17] and it is clear that only measurements at volume fractions above the postulated cluster glass transition line would be able to unambiguously demonstrate the existence of a truly arrested and nonergodic state at these concentrations. Unfortunately, it was not possible to directly reach the glass transition using the aforementioned method since the tracer particle addition inferred a finite sample dilution. In order to circumvent this we introduce another microrheology approach, CLSM-based MPT, for which we will later discuss a novel preparation method allowing us to reach the glass transition. Since the motion of the particles is captured in videos obtained via CLSM, the only requirement is that tracer particles are resolvable and fluorescent. As it is a more local measurement opposed to the bulk measurements obtained with DLS, the sample can also be checked for crystallites, local heterogeneities, and possible clustering of the tracer particles. An extra benefit is also obtained as even less sample volume is needed (5 μL).

The videos from CLSM are analyzed using standard particle tracking scripts, from which the time averaged 2D ($\langle \Delta x^2 + \Delta y^2 \rangle$) mean squared displacement (MSD) of each tracer particle is obtained, which are then ensemble averaged to yield a representative MSD of the sample.[34] All 2D-MSD MPT data are converted to 3D-MSD,[37] to match the dimensionality of the MSD calculated from DLS.[38] Note that while DLS in principle measures Brownian motion of the tracer particles along the direction of the scattering vector, the scattering of our system is completely isotropic, and the calculated MSD thus corresponds to the true 3D-MSD (throughout the rest of the text MSD will refer to 3D-MSD).

The slope of the 2D-MSD from MPT can easily be related to the diffusion coefficient D of the particles as $\langle \Delta x^2 + \Delta y^2 \rangle = 4D\tau + (V\tau)$,[2] where τ is the lag time, and V is overall drift.[37] However, extracting diffusion coefficients from the slope of the MSD determined by CLSM-based MPT data is not a very robust procedure—low statistics can alter the slope significantly, and the particular choice of cutoff values used to select the data range can be critical. Therefore, we have chosen a more robust approach as described in Josephson et al.[35,37] which we detailed in the Materials and Methods. In short, via the one-dimensional Van Hove self-correlation function $P(\Delta x, \tau)$ we test at which lag time τ the system displays purely diffusive motion with highest statistics, and use the selected data set to calculate the diffusion coefficient. We also perform a direct comparison of the measured MSDs from DLS and MPT, thus establishing that we are following tracer particle motion in the correct long time limit and that all particle displacements used to calculate D follow purely diffusive motion. The diffusion coefficient is then used together with the Stokes−Einstein relation to obtain the sample viscosity.

The validity of the MPT-approach is first confirmed by investigating conventionally prepared samples utilizing both MPT and DLS. The obtained viscosities are displayed together in Figure 1 and the results from both methods are consistent over the investigated concentration regime. The corresponding MSDs are shown in Figure 2a, which displays the expected overlap between the two techniques. For clarity, only a subset of samples is displayed in these figures with the entire sample set being available in the Supporting Information, Figures S2 and S3. As an example, typical Van Hove self-correlation functions at $\tau = 0.02$ s are shown in Figure 2b, although we note that different time steps τ were used for extraction of the

DOI: 10.1021/acs.jpcb.8b11781
J. Phys. Chem. B 2019, 123, 2432−2438

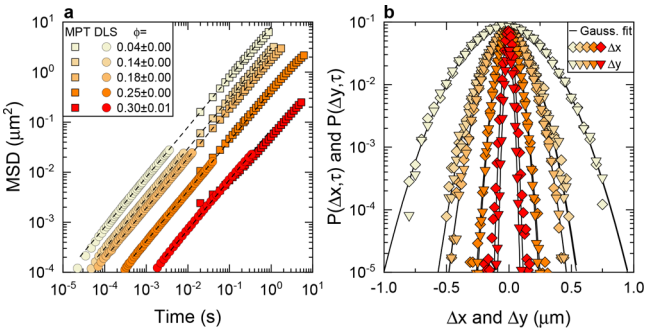

Figure 2. (a) mean squared displacements of tracer particles at different lysozyme concentration obtained using MPT (squares) and DLS (circles). The color scale indicates an increasing lysozyme concentration and corresponds to the same colored data points in Figure 1. Dashed lines indicate a purely diffusive system. The full data set is available in the Supporting Information, Figure S3. b) The Van Hove self-correlation functions at $\tau = 0.02$ s in both x and y direction (diamonds respectively upside down triangles). The diffusion coefficient of tracer particles was calculated using Gaussian fits (solid lines) to the Van Hove function. The color scale for the lysozyme concentration is the same as in Figure 1a.

viscosity values shown in Figure 1. All distributions follow a Gaussian distribution, confirming that the tracer particle motion is purely diffusive at all protein concentrations. This purely diffusive motion is also confirmed to be true for the DLS-measurements, as shown in the Supporting Information (Figure S4). A slowing down of the tracer particle motion at increasing lysozyme concentration is clearly seen, as the probability density function narrows with increasing volume fraction. Using the method described by Horn et al.,[39] we finally fit the data in Figure 1 using an effective hard sphere model (Quemada),[40] $\eta_r = (1 - \phi/\phi_{max})^{-2}$, in order to determine the critical volume fraction ϕ_{max} for the arrest transition. This results in a value of $\phi_{max} = 0.34$ for the liquid−solid transition of the system. Here we also note that this result is quite insensitive to the choice of the relationship used to fit the data for the concentration dependence of the reduced viscosity, which is demonstrated in Figure S2 in the Supporting Information, where we also include an analysis using the Krieger−Dougherty relation (KD), leading to $\phi_{max} = 0.35$.

Having confirmed the validity of MPT to obtain reliable values of the relative viscosity for lysozyme samples below the arrest line, we now attempt to experimentally verify the existence of a true cluster glass transition. The relative viscosity results (Figure 1) predict the glass transition to occur around $\phi = 0.34$. However, such high concentrations were impossible to create using standard sample preparation procedures. Therefore, we employed a simple but unconventional technique, where the concentration of a conventionally prepared protein sample (369 mg/mL; $\phi = 0.27$) is increased through controlled evaporation of water. The change in Hepes buffer concentration upon evaporation is expected to have a negligible effect on the low ionic strength conditions of the sample. This is due to it being a zwitterionic compound, the like of which are known to not contribute to the ionic strength of a solution.[41] Furthermore, there are no other components in the buffer that could affect the sample condition as great care is taken to remove any residual salt originating from the lysozyme powder during sample preparation. The final average sample concentration could then be gravimetrically determined from the reduced solvent content (Supporting Information, Figure S5). Several samples over a range of elevated concentrations were characterized using MPT. Five videos were created for each sample at distinctly different positions in an effort to explore the full sample volume.

The sample cell used for this controlled evaporation experiment consists of a microscope glass slide with a double-sided sticker that also acts as a spacer between glass slide and coverslip. The sticker possesses a hole in the middle where the sample droplet is deposited. Volumes of 5 μL were placed on the glass slide, and the evaporation was terminated by carefully pressing a coverslip on top in order to seal the cell. During evaporation, the initially homogeneous sample drop develops a macroscopically visible core−shell structure. A more concentrated shell forms at the air-sample interface, restricting evaporation of the inner more liquid core. This behavior is analogous to what has been observed in complex aqueous solutions,[42,43] where an intermediate state was observed with a solid shell at the air-sample interface and a liquid core. Sealing the cell with the coverslip induces a shearing force that effectively homogenizes the core−shell concentration profile present after the evaporation process, and the sample now looks again macroscopically homogeneous. It is worth mentioning that noticeably more force is required when sealing samples that are completely arrested. We highlight that this intermediate state appeared already after 2 min of evaporation, a time window that would rapidly decrease with higher starting concentrations. This could thus easily affect MPT−microrheology measurements that rely on handling minute sample volumes. In contrast, an immediately sealed sample shows no reduction in weight over the span of 7.5 h, corroborating that sealing indeed prevents further evaporation.

The recorded motion of the tracer particles, in the form of MSDs, is shown in Figure 3. The ensemble averaged MSD for each different sample location is displayed (i.e., each MSD represents one recorded video), to visualize the changes in the sample and highlight its heterogeneous nature as it approaches the glass transition. Each MSD corresponds to an individual observation volume, defined by the field of view for each frame 51.67 × 25.83 μm. At short evaporation times, all MSDs overlap, indicating a homogeneous sample in the liquid phase (Figure 3a,b). The averaged relative viscosity obtained from these state points have been included in Figure 1 and show good agreement with the conventionally prepared samples, which further supports the case that evaporation does not impact the sample behavior due to the great care taken during sample preparation to maintain a buffer condition corresponding to minimal ionic strength. This confirms the homogeneity of these samples, and that the overall concentration measured experimentally indeed characterizes all state points investigated within the sample. A heterogeneous slowing down occurs in the intermediate sample concentrations close to the arrest (Figure 3c,d), reflecting the existence of a concentration gradient from the liquid core to the solid shell within the sample. This inhomogeneity is only seen in the particle motion and not in the particle distribution, which remains homogeneous at all times. The reason why we see these concentration inhomogeneities in MPT experiments is the dramatic dependence of the viscosity on concentration close to the arrest transition, where η_r appears to diverge. This amplifies the effect of small inhomogeneities in concentration on the mobility of individual tracer particles, and it is thus reflected in the ensemble averaged MSDs shown in Figure 3c,d. Finally, once

DOI: 10.1021/acs.jpcb.8b11781
J. Phys. Chem. B 2019, 123, 2432−2438

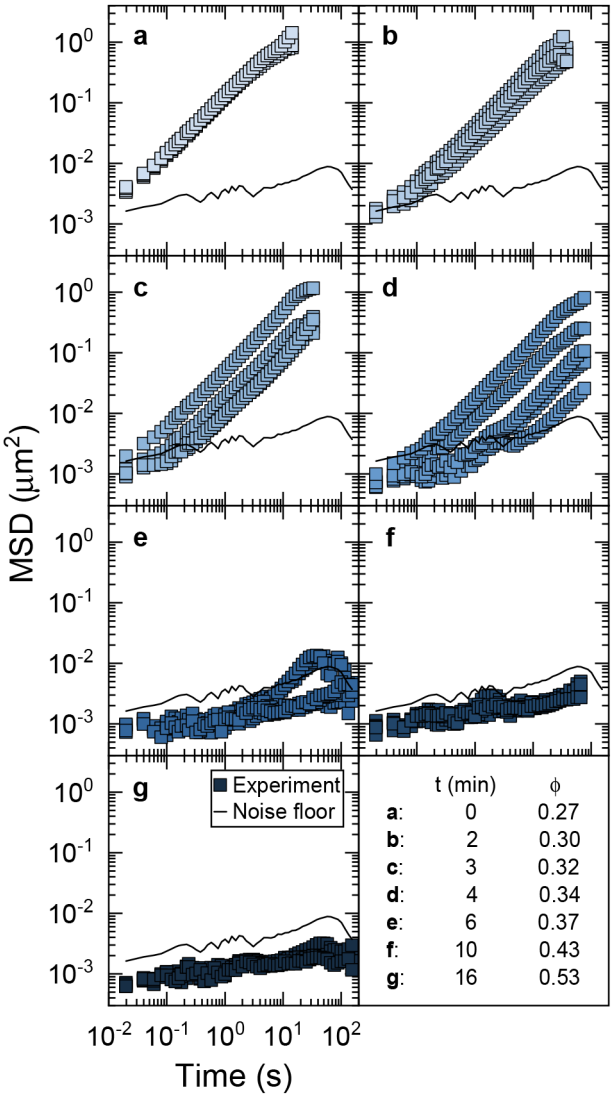

Figure 3. MSDs of tracer particles in lysozyme samples obtained using MPT (squares) at different evaporation times (increasing from a to g) displaying the entire range from liquid to solid behavior. Individual MSDs from measurements at different locations within the sample interior are shown. This illuminates the heterogeneity also observed macroscopically in the intermediate concentration regime. Displayed is also the noise floor obtained by fixating particles in a polymer matrix (solid line). The concentrations are estimated averages assuming a homogeneous evaporation rate throughout the entire sample.

the entire sample is completely arrested throughout, we lose any ability to detect still existing inhomogeneities as all tracer particles are now completely arrested within the spatial resolution of the confocal microscope on all accessible time scales, and their individual MSDs only reflect the instrument drift and thus once again overlap (Figure 3e,f). The averaged lysozyme volume fraction at which the glass transition occurs is thus around ϕ_{max} = 0.34−0.37, in line with the results from the Quemada fit (ϕ_{max} = 0.34).

The observed arrest thus supports the prediction by Cardinaux et al.[14] regarding the existence of a cluster glass transition in a low ionic strength lysozyme system. While their exact location of the arrest transition differs from that presented here, the lower volume fraction predicted for the glass transition at 5 °C as compared to our results (20 °C) can at least partially be rationalized by the known enhancement of cluster growth at lower temperatures.[14] In fact, the relative viscosity results shown in Figure 1 correspond reasonably well with the data presented by Godfrin et al.[17] despite the differences in sample preparation/condition (Supporting Information, Figure S6). We can only speculate as to what may have led to the different conclusion drawn by Godfrin et al.,[17] who stated that lysozyme remains a macroscopic fluid even at high protein concentrations based on their active microrheology experiments. A possibility could be the sensitivity of the system, with respect to its interaction potential and the resulting cluster size distribution, to pH and ionic content.[9,15,17,18,44,45] Additionally, it has been established that lysozyme responds differently to active versus passive microrheology.[46,47] Perhaps the soft cluster glass, that forms as a result of the weak temporary bonds induced by the SALR potential, locally shear-melts already at the low shear stress induced by the active microrheology experiment.

CONCLUSIONS

In conclusion, the cluster glass transition in concentrated lysozyme samples has been characterized through a combination of microrheology (which allows for minute sample volumes) and controlled evaporation (which lead to concentrations beyond the glass transition). Our experiments unambiguously demonstrate that full arrest occurs around ϕ_{max} = 0.34−0.37. The relative viscosities determined by DLS and MPT-based microrheology quantitatively agree throughout the fluid regime, and their concentration dependence is reproduced by the Quemada relationship, predicting an arrest transition at ϕ_{max} = 0.34, in agreement with the findings from the controlled evaporation experiments. This study showcases how one can explore previously unreachable regions, at and beyond arrest transitions, of concentrated protein solutions using such microliter-based approaches. Future work should include mapping the arrest line of lysozyme as a function of pH and ionic strength, where controlled evaporation could shed light on the phase behavior of lysozyme in the transition regime between salt-free conditions and high ionic strength. Another open question is the effect of induced stress on local microrheological properties of the cluster glass, and the relation of induced stress to the existence of a macroscopic yield stress value, which could be pursued using a combination of classical rheometry and active microrheology. As a side-note, we also caution others to account for the possible concentration increase caused by evaporation during the short period before the sample is properly sealed, which can be highly significant when performing microrheology experiments on concentrated samples close to an arrest transition using microliter volumes.

ASSOCIATED CONTENT

Supporting Information

The Supporting Information is available free of charge on the ACS Publications website at DOI: 10.1021/acs.jpcb.8b11781.

Additional information regarding functionalization verification and evaporation procedure, full data set of the investigated lysozyme samples and comparison with literature, and complementary information regarding the validity of DLS-MSD. (PDF)

DOI: 10.1021/acs.jpcb.8b11781
J. Phys. Chem. B 2019, 123, 2432−2438

AUTHOR INFORMATION

Corresponding Author

*(A.S.) E-mail: anna.stradner@fkem1.lu.se.

ORCID

Maxime J. Bergman: 0000-0002-5803-8517
Tommy Garting: 0000-0002-9423-1031
Peter Schurtenberger: 0000-0002-2790-8831
Anna Stradner: 0000-0003-3310-3412

Author Contributions

M.J.B. and T.G. contributed equally to this work.

Notes

The authors declare no competing financial interest.

ACKNOWLEDGMENTS

This work was supported by the Knut and Alice Wallenberg Foundation (Project Grant KAW 2014.0052). P.S. acknowledges financial support from the European Research Council (ERC-339678-COMPASS). A.S. acknowledges financial support from the Swedish Research Council (VR Grant 2016-03301) and the Faculty of Science at Lund University.

REFERENCES

(1) Stradner, A.; Sedgwick, H.; Cardinaux, F.; Poon, W. C. K.; Egelhaaf, S. U.; Schurtenberger, P. Equilibrium Cluster Formation in Concentrated Protein Solutions and Colloids. *Nature* **2004**, *432*, 492−495.

(2) Yearley, E. J.; Godfrin, P. D.; Perevozchikova, T.; Zhang, H.; Falus, P.; Porcar, L.; Nagao, M.; Curtis, J. E.; Gawande, P.; Taing, R.; et al. Observation of Small Cluster Formation in Concentrated Monoclonal Antibody Solutions and its Implications to Solution Viscosity. *Biophys. J.* **2014**, *106*, 1763−1770.

(3) Liu, J.; Nguyen, M. D. H.; Andya, J. D.; Shire, S. J. Reversible Self-Association Increases the Viscosity of a Concentrated Monoclonal Antibody in Aqueous Solution. *J. Pharm. Sci.* **2005**, *94*, 1928−1940.

(4) Galkin, O.; Pan, W.; Filobelo, L.; Hirsch, R. E.; Nagel, R. L.; Vekilov, P. G. Two-Step Mechanism of Homogeneous Nucleation of Sickle Cell Hemoglobin Polymers. *Biophys. J.* **2007**, *93*, 902−913.

(5) Pan, W.; Galkin, O.; Filobelo, L.; Nagel, R. L.; Vekilov, P. G. Metastable Mesoscopic Clusters in Solutions of Sickle-Cell Hemoglobin. *Biophys. J.* **2007**, *92*, 267−277.

(6) Liu, Y.; Fratini, E.; Baglioni, P.; Chen, W.-R.; Chen, S.-H. Effective Long-Range Attraction Between Protein Molecules in Solution Studied by Small Angle Neutron Scattering. *Phys. Rev. Lett.* **2005**, *95*, 118102.

(7) Stradner, A.; Cardinaux, F.; Schurtenberger, P. Comment on "Effective Long-Range Attraction Between Protein Molecules in Solution Studied by Small Angle Neutron Scattering". *Phys. Rev. Lett.* **2006**, *96*, 219801.

(8) Stradner, A.; Cardinaux, F.; Schurtenberger, P. A Small-Angle Scattering Study on Equilibrium Clusters in Lysozyme Solutions. *J. Phys. Chem. B* **2006**, *110*, 21222−21231.

(9) Cardinaux, F.; Stradner, A.; Schurtenberger, P.; Sciortino, F.; Zaccarelli, E. Modeling Equilibrium Clusters in Lysozyme Solutions. *Europhys. Lett.* **2007**, *77*, 48004.

(10) Liu, Y.; Porcar, L.; Chen, J.; Chen, W.-R.; Falus, P.; Faraone, A.; Fratini, E.; Hong, K.; Baglioni, P. Lysozyme Protein Solution with an Intermediate Range Order Structure. *J. Phys. Chem. B* **2011**, *115*, 7238−7247.

(11) Porcar, L.; Falus, P.; Chen, W.-R.; Faraone, A.; Fratini, E.; Hong, K.; Baglioni, P.; Liu, Y. Formation of the Dynamic Clusters in Concentrated Lysozyme Protein Solutions. *J. Phys. Chem. Lett.* **2010**, *1*, 126−129.

(12) Barhoum, S.; Yethiraj, A. NMR Detection of an Equilibrium Phase Consisting of Monomers and Clusters in Concentrated Lysozyme Solutions. *J. Phys. Chem. B* **2010**, *114*, 17062−17067.

(13) Kowalczyk, P.; Ciach, A.; Gauden, P. A.; Terzyk, A. P. Equilibrium Clusters in Concentrated Lysozyme Protein Solutions. *J. Colloid Interface Sci.* **2011**, *363*, 579−584.

(14) Cardinaux, F.; Zaccarelli, E.; Stradner, A.; Bucciarelli, S.; Farago, B.; Egelhaaf, S. U.; Sciortino, F.; Schurtenberger, P. Cluster-Driven Dynamical Arrest in Concentrated Lysozyme Solutions. *J. Phys. Chem. B* **2011**, *115*, 7227−7237.

(15) Falus, P.; Porcar, L.; Fratini, E.; Chen, W.-R.; Faraone, A.; Hong, K.; Baglioni, P.; Liu, Y. Distinguishing the Monomer to Cluster Phase Transition in Concentrated Lysozyme Solutions by Studying the Temperature Dependence of the Short-Time Dynamics. *J. Phys.: Condens. Matter* **2012**, *24*, No. 064114.

(16) Godfrin, P. D.; Valadez-Pérez, N. E.; Castañeda-Priego, R.; Wagner, N. J.; Liu, Y. Generalized Phase Behavior of Cluster Formation in Colloidal Dispersions with Competing Interactions. *Soft Matter* **2014**, *10*, 5061−5071.

(17) Godfrin, P. D.; Hudson, S. D.; Hong, K.; Porcar, L.; Falus, P.; Wagner, N. J.; Liu, Y. Short-Time Glassy Dynamics in Viscous Protein Solutions with Competing Interactions. *Phys. Rev. Lett.* **2015**, *115*, 228302.

(18) Riest, J.; Nägele, G.; Liu, Y.; Wagner, N. J.; Godfrin, P. D. Short-Time Dynamics of Lysozyme Solutions with Competing Short-Range Attraction and Long-Range Repulsion: Experiment and Theory. *J. Chem. Phys.* **2018**, *148*, No. 065101.

(19) Baumketner, A.; Cai, W. Clusters of Lysozyme in Aqueous Solutions. *Phys. Rev. E: Stat. Phys., Plasmas, Fluids, Relat. Interdiscip. Top.* **2018**, *98*, No. 032419.

(20) Furst, E. M.; Squires, T. M. *Microrheology*; Oxford University Press: Oxford, U.K., 2017.

(21) Zia, R. N. Active and Passive Microrheology Theory and Simulation. *Annu. Rev. Fluid Mech.* **2018**, *50*, 371−405.

(22) Pan, W.; Filobelo, L.; Pham, N. D. Q.; Galkin, O.; Uzunova, V. V.; Vekilov, P. G. Viscoelasticity in Homogeneous Protein Solutions. *Phys. Rev. Lett.* **2009**, *102*, No. 058101.

(23) Bauer, K. C.; Schermeyer, M.-T.; Seidel, J.; Hubbuch, J. Impact of Polymer Surface Characteristics on the Microrheological Measurement Quality of Protein Solutions - A Tracer Particle Screening. *Int. J. Pharm.* **2016**, *505*, 246−254.

(24) Escobedo-Sánchez, M. A.; Segovia-Gutiérrez, J. P.; Zuccolotto-Bernez, A. B.; Hansen, J.; Marciniak, C. C.; Sachowsky, K.; Platten, F.; Egelhaaf, S. U.; et al. Microliter Viscometry Using a Bright-Field Microscope: n-DDM. *Soft Matter* **2018**, *14*, 7016−7025.

(25) Garting, T.; Stradner, A. Optical Microrheology of Protein Solutions Using Tailored Nanoparticles. *Small* **2018**, *14*, 1801548.

(26) Mason, T. G.; Ganesan, K.; van Zanten, J. H.; Wirtz, D.; Kuo, S. C. Particle Tracking Microrheology of Complex Fluids. *Phys. Rev. Lett.* **1997**, *79*, 3282−3285.

(27) Gisler, T.; Weitz, D. A. Tracer Microrheology in Complex Fluids. *Curr. Opin. Colloid Interface Sci.* **1998**, *3*, 586−592.

(28) Wilson, L. G.; Harrison, A. W.; Schofield, A. B.; Arlt, J.; Poon, W. C. K. Passive and Active Microrheology of Hard-Sphere Colloids. *J. Phys. Chem. B* **2009**, *113*, 3806−3812.

(29) Urban, C.; Schurtenberger, P. Characterization of Turbid Colloidal Suspensions Using Light Scattering Techniques Combined with Cross-Correlation Methods. *J. Colloid Interface Sci.* **1998**, *207*, 150−158.

(30) Pusey, P. N. Suppression of Multiple Scattering by Photon Cross-Correlation Techniques. *Curr. Opin. Colloid Interface Sci.* **1999**, *4*, 177−185.

(31) Block, I. D.; Scheffold, F. Modulated 3D Cross-Correlation Light Scattering: Improving Turbid Sample Characterization. *Rev. Sci. Instrum.* **2010**, *81*, 123107.

(32) Koppel, D. E. Analysis of Macromolecular Polydispersity in Intensity Correlation Spectroscopy: The Method of Cumulants. *J. Chem. Phys.* **1972**, *57*, 4814−4820.

DOI: 10.1021/acs.jpcb.8b11781
J. Phys. Chem. B 2019, 123, 2432−2438

(33) Frisken, B. J. Revisiting the Method of Cumulants for the Analysis of Dynamic Light- Scattering Data. *Appl. Opt.* **2001**, *40*, 4087−4091.
(34) Crocker, J. C.; Grier, D. G. Methods of Digital Video Microscopy for Colloidal Studies. *J. Colloid Interface Sci.* **1996**, *179*, 298−310.
(35) Josephson, L. L.; Furst, E. M.; Galush, W. J. Particle Tracking Microrheology of Protein Solutions. *J. Rheol.* **2016**, *60*, 531−540.
(36) Valentine, M. T.; Kaplan, P. D.; Thota, D.; Crocker, J. C.; Gisler, T.; Prud'homme, R. K.; Beck, M.; Weitz, D. A. Investigating the Microenvironments of Inhomogeneous Soft Materials with Multiple Particle Tracking. *Phys. Rev. E: Stat. Phys., Plasmas, Fluids, Relat. Interdiscip. Top.* **2001**, *64*, No. 061506.
(37) Moschakis, T. Microrheology and Particle Tracking in Food Gels and Emulsions. *Curr. Opin. Colloid Interface Sci.* **2013**, *18*, 311−323.
(38) Amin, S.; Blake, S.; Kenyon, S. M.; Kennel, R. C.; Lewis, E. N. A Novel Combination of DLS-Optical Microrheology and Low Frequency Raman Spectroscopy to Reveal Underlying Biopolymer Self-Assembly and Gelation Mechanisms. *J. Chem. Phys.* **2014**, *141*, 234201.
(39) Horn, F. M.; Richtering, W.; Bergenholtz, J.; Willenbacher, N.; Wagner, N. J. Hydrodynamic and Colloidal Interactions in Concentrated Charge-Stabilized Polymer Dispersions. *J. Colloid Interface Sci.* **2000**, *225*, 166−178.
(40) Quemada, D. Rheology of Concentrated Disperse Systems and Minimum Energy Dissipation Principle - I. Viscosity-Concentration Relationship. *Rheol. Acta* **1977**, *16*, 82−94.
(41) Stellwagen, E.; Prantner, J. D.; Stellwagen, N. C. Do Zwitterions Contribute to the Ionic Strength of a Solution? *Anal. Biochem.* **2008**, *373*, 407−409.
(42) Roger, K.; Liebi, M.; Heimdal, J.; Pham, Q. D.; Sparr, E. Controlling Water Evaporation Through Self-Assembly. *Proc. Natl. Acad. Sci. U. S. A.* **2016**, *113*, 10275−10280.
(43) Roger, K.; Sparr, E.; Wennerström, H. Evaporation, Diffusion and Self-Assembly at Drying Interfaces. *Phys. Chem. Chem. Phys.* **2018**, *20*, 10430−10438.
(44) Gibaud, T.; Schurtenberger, P. A Closer Look at Arrested Spinodal Decomposition in Protein Solutions. *J. Phys.: Condens. Matter* **2009**, *21*, 322201.
(45) Gibaud, T.; Cardinaux, F.; Bergenholtz, J.; Stradner, A.; Schurtenberger, P. Phase Separation and Dynamical Arrest for Particles Interacting with Mixed Potentials - the Case of Globular Proteins Revisited. *Soft Matter* **2011**, *7*, 857−860.
(46) Dharmaraj, V. L.; Godfrin, P. D.; Liu, Y.; Hudson, S. D. Rheology of Clustering Protein Solutions. *Biomicrofluidics* **2016**, *10*, No. 043509.
(47) Allan, D. B.; Firester, D. M.; Allard, V. P.; Reich, D. H.; Stebe, K. J.; Leheny, R. L. Linear and Nonlinear Microrheology of Lysozyme Layers Forming at the Air-Water Interface. *Soft Matter* **2014**, *10*, 7051−7060.

DOI: 10.1021/acs.jpcb.8b11781
J. Phys. Chem. B 2019, 123, 2432−2438